

# PFGE: Parsimonious Fast Geometric Ensembling of DNNs

Hao Guo<sup>1</sup> Jiyong Jin<sup>1</sup> Bin Liu<sup>1</sup>

## Abstract

Ensemble methods have been widely used to improve the performance of machine learning methods in terms of generalization and uncertainty calibration, while they struggle to use in deep learning systems, as training an ensemble of deep neural networks (DNNs) and then deploying them for online prediction incur an extremely higher computational overhead of model training and test-time predictions. Recently, several advanced techniques, such as fast geometric ensembling (FGE) and snapshot ensemble, have been proposed. These methods can train the model ensembles in the same time as a single model, thus getting around the hurdle of training time. However, their overhead of model recording and test-time computations remains much higher than their single model based counterparts. Here we propose a parsimonious FGE (PFGE) that employs a lightweight ensemble of higher-performing DNNs generated by several successively-performed procedures of stochastic weight averaging. Experimental results across different advanced DNN architectures on different datasets, namely CIFAR- $\{10, 100\}$  and Imagenet, demonstrate its performance. Results show that, compared with state-of-the-art methods, PFGE achieves better generalization performance and satisfactory calibration capability, while the overhead of model recording and test-time predictions is significantly reduced. Our code is available at <https://github.com/ZJLAB-AMMI/PFGE>.

## 1. Introduction

Ensembling methods have been widely used to improve the generalization performance of machine learning methods (Dietterich, 2000; Zhou, 2012; Caruana et al., 2004;

<sup>1</sup>Research Center for Applied Mathematics and Machine Intelligence, Zhejiang Lab, Hangzhou, Zhejiang, China. Correspondence to: Bin Liu <liubin@zhejianglab.com; bins@ieee.org>.

Džeroski & Ženko, 2004). However, they struggle to apply in learning with modern deep neural networks (DNNs). A modern DNN often has millions, even billions, of parameters, see e.g., (Beal et al., 2022). A direct ensembling of  $k$  DNNs leads to a  $k$ -folded computational overhead in terms of training time, memory requirement, and test-time prediction.

Nevertheless, important advances have been made recently in adapting the idea of ensembling to improve deep learning. For instance, the fast geometric ensembling (FGE) and snapshot ensemble (SNE) methods can train an ensemble of DNNs in the same time as a single model, thus getting around the hurdle of training time (Garipov et al., 2018; Huang et al., 2017a). However, their computational overhead of training-time model recording and test-time predictions remain much higher than their single model based counterparts. To reduce the test-time cost of ensembles, (Bucilua et al., 2006; Hinton et al., 2015) propose methods for model compression and knowledge distillation, which aim to train one single model to encompass the “knowledge” of the ensembles. However, such methods do not consider the computational overhead due to ensemble training. For the aforementioned methods, the computational overhead remains prohibitively high for many real-life applications with limited budgets for saving and deploying the model ensembles.

In this paper, we present PFGE, a parsimonious version of FGE, which aims to reduce both the training-time and the test-time computational overhead yielded from DNNs ensembling. Compared with state-of-the-art (SOTA) methods, PFGE achieves better generalization performance and satisfactory calibration capability, while the computational overhead of model recording and test-time predictions is significantly reduced. The design of PFGE is inspired by an observation of that running one time of stochastic weight averaging (SWA) procedure can lead to a wider optimum (Izmailov et al., 2018), and performing a series of SWA procedures successively could find a set of higher-performing weights than those obtained by stochastic gradient descend (SGD) (Guo et al., 2022). FGE employs an ensemble of models found by SGD. We expect that, by employing an ensemble of higher-performing models found by SWA, PFGE could use much fewer model ensembles to yield a comparable performance with FGE.

As PFGE reduces both the training and test-time computational overhead without a compromise in generalization, we believe that the appearance of PFGE can remove the obstacle to a large extent in applying ensemble methods for diverse DNN applications.

Our contributions can be summarized as follows:

- We propose a novel, generic, and architecture-agnostic ensemble-based algorithm, referred to as PFGE, for improving DNNs in terms of generalization and calibration. PFGE maintains the full advantage of FGE in high training efficiency and desirable generalization performance, while remarkably reduces its computational overhead of model recording and test-time predictions. To our knowledge, PFGE is by far the only ensemble-based algorithm that targets reducing both the training and test-time computational overhead yielded from DNN ensembling.
- We empirically demonstrate that employing higher-performing DNNs is an effective strategy for reducing the requirement on the number of models for ensemble-based deep learning.
- We propose a novel SWA-based approach to generate higher-performing models, in terms of generalization and mode connectivity, for ensemble-based deep learning.
- We perform extensive experiments to test the performance of our algorithm. Results show a multifaceted advantage of our algorithm over competitors, including a better balance between generalization, calibration and computational overhead, the capability of generating model components with better generalization and mode connectivity.

## 2. Related Works

### Optimization algorithms for training DNNs

SGD is by far the *de facto* optimization approach to train DNNs. A decaying learning rate (LR) is the standard configuration for SGD. A commonly used strategy for improving SGD in terms of generalization is to design better LRs. For instance, the AdaGrad method estimates the LR online from the gradients (Duchi et al., 2011). AdaGrad is further improved in (Kingma & Ba, 2014), where the resulting algorithm is referred to as AdaDelta. The Adam algorithm is proposed in (Kingma & Ba, 2014), which combines the advantages of AdaGrad and RMSProp (Tieleman & Hinton, 2012). In (Schaul et al., 2013), the diagonal approximation of the Hessian of the gradients is used for designing adaptive LRs. As the literature on this topic is vast, we could not enumerate due to space limitation. We refer interested

readers to (Sun, 2019) and references therein for more details.

The above optimization-based approaches are all single model based. In this paper, we focus on ensemble methods that is featured by the application of multiple models for improving DNN performance in terms of generalization and calibration.

### Bayesian methods for learning with neural networks

Since the seminal works of (Neal, 2012; MacKay, 1992), Bayesian methods have been extensively investigated in neural network based machine learning. Such methods have desirable theoretical properties, especially in terms of uncertainty qualification. However, they are largely computationally intractable when facing modern DNNs, due to an extremely high dimension of the model parameter and a strong non-convexity of the posterior distribution.

(Neal, 2012) proposes Hamiltonian Monte Carlo (HMC), a powerful iterative sampling method that can handle non-convex posteriors, while it requires full gradients at each iteration, thus is computationally prohibitive for training with massive data points. A common wisdom used for training with large scale datasets is to iteratively train with mini-batch samples, which is scalable and able to discover good solution subspaces (Keskar et al., 2017). Stochastic gradient HMC (SGHMC) extends HMC by using mini-batch sample based stochastic gradients (Chen et al., 2014). (Welling & Teh, 2011) introduces the first order Langevin dynamics into the framework of stochastic gradient based Markov Chain Monte Carlo setting (SG-MCMC). (Mandt et al., 2017) provide a theoretical tie that connects SG-MCMC to SGD and its variants, and analyze their approximation errors.

Outside of MCMC, variational inference and sequential Monte Carlo methods are also explored for large scale training, see e.g., (Hoffman et al., 2013; Graves, 2011; Liu, 2020), while it is quite difficult for balancing computational efficiency with approximation errors when adapting them to modern DNNs.

Our PFGE algorithm acts as a much more computationally efficient subspace-based posterior sampling approach, which is applicable for modern DNNs. Its desirable performance in terms of computational efficiency, generalization, and calibration is due to a novel algorithm design that combines SWA and FGE, which makes full use of recently revealed geometric insights regarding the DNN loss landscape.

### Ensembling methods adapted to DNNs

As aforementioned, ensemble methods are often computationally intractable for learning with modern DNNs, due to an extremely high overhead of ensem-

ble training, model recording, and test-time predictions. Nevertheless, notable advances have been made to adapt ensemble methods to DNNs, such as FGE (Garipov et al., 2018), SNE (Huang et al., 2017a), SWA-Gaussian (SWAG) (Maddox et al., 2019), Monte-Carlo dropout (Gal & Ghahramani, 2016), and deep ensembles (Fort et al., 2019; Lakshminarayanan et al., 2017b). Among these modern approaches, FGE, SNE and SWAG are most related to this work, as they all employ a cyclical LR to generate the model ensembles in the same time as one single model.

Both FGE and SNE build DNN ensembles by sampling network weights from an SGD trajectory corresponding to a cyclical LR (Smith, 2017). Running an SGD with a cyclical LR is in principle equivalent to SGD sampling with periodic warm restarts (Loshchilov & Hutter, 2017). (Huang et al., 2017a; Garipov et al., 2018) demonstrate that the cyclical LR indeed provides a highly efficient way to collect high-quality DNN weights, which define the models for ensembling.

Compared with SNE, FGE is featured by a geometric explanation of its way to generating the ensembles. Specifically, FGE is inspired by one geometric insight about the DNN loss landscape, which says that there exist simple curves that connect local optima of the DNN loss landscape, and over these curves, both the training accuracy and the test accuracy remain approximately constant. FGE provides an efficient way to discover the high-accuracy pathways between local optima.

Inspired by FGE, SWA is proposed, which averages the high-performing network weights yielded by FGE for test-time inference (Izmailov et al., 2018). The geometric insight underlying SWA is that averaging weights along an SGD trajectory corresponding to a cyclical or constant LR can find wider optima, and wider optima lead to better generalization. This insight is questioned by (Guo et al., 2022), which shows that the real function of SWA’s weight averaging operation lies in reducing the variance of the final output, similarly to tail-averaging (Prateek et al., 2018).

SWAG uses the SWA solution as the center of a Gaussian distribution, which is formed to approximate the posterior of the network weights (Maddox et al., 2019). SWAG generates the model ensembles by sampling from this Gaussian.

PFGE represents a novel SOTA algorithm for ensemble-based deep learning, featured by its competitive performance, in terms of generalization and calibration, compared with related SOTA methods, and a much-reduced computational overhead of memory and test-time predictions.

### Uncertainty calibration for DNNs

---

**Algorithm 1** SWA based model training and test-time prediction

---

**Input:** initial network weights  $w_0$ , cyclical LR schedule  $SC$ , cycle length  $c$ , budget (the total number of allowable iterations)  $n$ , test data  $x$

**Output:** predicted label  $y$  of  $x$

```

1:  $w \leftarrow w_0$ ; solution set  $\mathcal{S} \leftarrow \{\}$ .
2:  $w_{\text{SWA}} \leftarrow w$ .
3: for  $i \leftarrow 1, 2, \dots, n$  do
4:   Compute current learning rate  $\alpha$  according to  $SC$ .
5:    $w \leftarrow w - \alpha \bigtriangledown \mathcal{L}_i(w)$  (stochastic gradient update).
6:   if  $\text{mod}(i,c)=0$  then
7:      $n_{\text{models}} \leftarrow i/c$  (number of models averaged).
8:      $w_{\text{SWA}} \leftarrow (w_{\text{SWA}} \cdot n_{\text{models}} + w) / (n_{\text{models}} + 1)$ .
9:   end if
10: end for
11: Input  $x$  into the DNN with weights  $w_{\text{SWA}}$ , then compute
     the its softmax output.
12: return  $y$  that maximizes the above softmax output.

```

---

**Algorithm 2** FGE based model training and test-time prediction

---

**Input:** initial network weights  $w_0$ , cyclical LR schedule  $SC$ , cycle length  $c$ , budget (the total number of allowable iterations)  $n$ , test data  $x$

**Output:** predicted label  $y$  of  $x$

```

1:  $w \leftarrow w_0$ ; solution set  $\mathcal{S} \leftarrow \{\}$ .
2: for  $i \leftarrow 1, 2, \dots, n$  do
3:   Compute current learning rate  $\alpha$  according to  $SC$ .
4:    $w \leftarrow w - \alpha \bigtriangledown \mathcal{L}_i(w)$  (stochastic gradient update).
5:   if  $\text{mod}(i,c)=0$  then
6:     Add  $w$  into  $\mathcal{S}$  (collect weights).
7:   end if
8: end for
9: Given  $x$  as the input, compute the average of softmax
   outputs of models included in  $\mathcal{S}$ .
10: return  $y$  that maximizes the above averaged softmax
    output.

```

---

Uncertainty calibration is crucially important for robust decision-making and model interpretability (Guo et al., 2017). It aims to provide a calibrated, more accurate confidence measure for each prediction provided by a DNN model.

Ensemble methods provide a natural mechanism for uncertainty calibration. (Maddox et al., 2019) suggests uncertainty calibration of DNNs via sampling from the Gaussian approximation to the posterior given by SWAG, and then doing Bayesian model averaging over those samples. (Lakshminarayanan et al., 2017a) propose incorporating an adversarial loss function into the ensemble for enhanced calibration.

Outside of ensemble methods, the rescaling techniques are commonly used for enhancing calibration. They work by rescaling the logits of DNN outputs (Guo et al., 2017; Kuleshov et al., 2018).

As an ensemble method, PFGE can be naturally used for uncertainty calibration. We test its calibration performance in Section 4.

### 3. The Proposed PFGE Algorithm

Our PFGE algorithm is developed based on SWA and FGE. We present the pseudo-codes to implement SWA, FGE, and PFGE in Algorithms 1, 2, and 3, respectively. They all perform stochastic gradient based weight updating iteratively, starting at a local optimum  $w_0$  given by a preceding SGD phase or a pre-trained DNN model.

**Algorithm 3** PFGE based model training and test-time prediction

**Input:** initial network weights  $w_0$ , cyclical LR schedule  $SC$ , cycle length  $c$ , budget (the total number of allowable iterations)  $n$ , test data  $x$ , model recording period  $P$

**Output:** predicted label  $y$  of  $x$

```

1:  $w \leftarrow w_0$ ; solution set  $\mathcal{S} \leftarrow \{\}$ .
2:  $w_{\text{SWA}} \leftarrow w$ .
3:  $n_{\text{recorded}} \leftarrow 0$  (number of models recorded in  $\mathcal{S}$ ).
4: for  $i \leftarrow 1, 2, \dots, n$  do
5:   Compute current learning rate  $\alpha$  according to  $SC$ .
6:    $w \leftarrow w - \alpha \bigtriangledown \mathcal{L}_i(w)$  (stochastic gradient update).
7:    $j \leftarrow i - n_{\text{recorded}} \times P$  (iterate index for the follow-up
      SWA procedure).
8:   if  $\text{mod}(j, c) = 0$  then
9:      $n_{\text{models}} \leftarrow j/c$  (number of models that have been
       averaged within the current SWA procedure).
10:     $w_{\text{SWA}} \leftarrow (w_{\text{SWA}} \cdot n_{\text{models}} + w) / (n_{\text{models}} + 1)$ .
11:   end if
12:   if  $\text{mod}(i, P) = 0$  then
13:     Add  $w_{\text{SWA}}$  into  $\mathcal{S}$  (collect weights).
14:      $w \leftarrow w_{\text{SWA}}$  (initialization for the follow-up SWA
       procedure).
15:      $n_{\text{recorded}} \leftarrow i/P$  (number of models recorded in  $\mathcal{S}$ ).
16:   end if
17: end for
18: Given  $x$  as the input, compute the average of softmax
   outputs of models recorded in  $\mathcal{S}$ .
19: return  $y$  that maximizes the above averaged softmax
   output.

```

The iterative weight updating operation employs a cyclical LR for letting the weight trajectory escape from the current optimum, and then discover and converge to novel local optima. A conceptual diagram of the cyclical LR is shown in Figure 1, where  $\alpha_1$  and  $\alpha_2$  bound the LR values,  $c$  denotes

the cycle length,  $n$  the total number of allowable iterations that define the budget of training time,  $P$  the model recording period for PFGE.

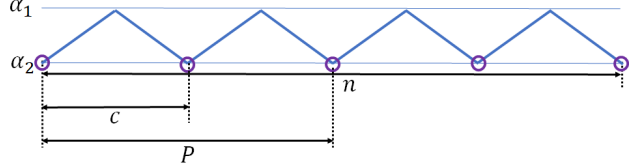


Figure 1. A conceptual diagram of the cyclical LR used by SWA, FGE and PFGE. The circles mask the time instances for recording the local optima discovered along the SGD trajectory. The real relationship between  $c$ ,  $P$ , and  $n$  is that  $P$  is an integer multiple of  $c$ , and  $n$  is an integer multiple of  $P$ . Here only one example case is plotted, in which  $P = 2c$  and  $n = 2P$ . See the text for detailed explanations for all parameters involved.

As shown in Algorithm 1, SWA maintains a running average of the network weights that are recorded at every  $c$  iterations, and finally outputs a single model with weight  $w_{\text{SWA}}$  for test-time prediction.  $w_{\text{SWA}}$  is in fact the average of  $(\frac{n}{c} + 1)$  weights traversed along the SGD trajectory.

As shown in Algorithm 2, FGE uses the same mechanism as SWA to find  $(\frac{n}{c} + 1)$  local optima. Different from SWA that uses the average of those local optima for test-time prediction, FGE maintains an ensemble of  $(\frac{n}{c} + 1)$  models defined by those local optima. Its test-time prediction is made based on the average of the model ensembles' softmax outputs. Compared with using one single DNN, using FGE requires  $(\frac{n}{c} + 1)$  times memory for recording the model components, and  $(\frac{n}{c} + 1)$  times computational overhead of test-time predictions. PFGE reduces the multiple number  $(\frac{n}{c} + 1)$  to  $(\frac{n}{P} + 1)$ . Note that  $P$  is integer multiples of  $c$ , as exemplifies in Figure 1.

PFGE differentiates with FGE in the way to generate the ensemble models. For FGE, its ensemble models are generated purely by SGD (see operations 4 and 6 in Algorithm 2), while PFGE resorts to multiple SWA operations performed in succession (see operations 10 and 13 in Algorithm 3) to generate the models. In the successively performed SWA procedures, the output of an SWA procedure is used to initialize its follow-up SWA procedure (see operation 14 in Algorithm 3).

The recently reported Double SWA (DSWA) and Triple SWA (TSWA) methods also use the strategy of performing multiple SWA procedures successively (Guo et al., 2022). Both DSWA and TSWA output a single model, while PFGE maintains an ensemble of multiple models, for test-time prediction.

As SWA is capable of finding local optima with better generalization (Izmailov et al., 2018), we replace the iterative SGD procedure in FGE with a series of successively performed SWA procedures for generating an ensemble of higher-performing models, yielding the PFGE algorithm. In the following section, we present experimental results, which demonstrate the desirable performance of PFGE in terms of generalization and calibration compared with SOTA methods.

## 4. Experiments

We compare PFGE against SOTA methods FGE (Garipov et al., 2018), SWA (Izmailov et al., 2018), and SWAG (Maddox et al., 2019), on CIFAR-10 (Krizhevsky & Hinton, 2009), CIFAR-100 (Krizhevsky & Hinton, 2009), and ImageNet ILSVRC-2012 (Deng et al., 2009; Russakovsky et al., 2015), to test its performance in terms of generalization and uncertainty calibration.

### 4.1. Experimental Setting

As shown in Algorithms 1-3, SWA, FGE, and PFGE are all initialized with a local optimum  $w_0$  and an LR schedule. For all architectures and datasets, we initialize all algorithms in comparison with the same  $w_0$ , and the same LR setting. Following (Garipov et al., 2018), we use a triangle LR schedule, as shown in Figure 1. Specifically, we set  $c$  to iteration numbers corresponding to 2 or 4 epochs (following (Garipov et al., 2018)),  $P$  to 10 epochs, and  $n$  to 40 or 20 epochs. For  $\alpha_1$ , and  $\alpha_2$ , we set them in the same way as in (Garipov et al., 2018). The mini-batch size for model training is fixed at 128.

For CIFAR- $\{10, 100\}$ , we obtain  $w_0$  from running a standard SGD with momentum affiliated by the same type of decaying LR schedule as used in (Izmailov et al., 2018), to minimize an  $L_2$ -regularization based cross-entropy loss, until convergence. We set the hyperparameters of SGD, e.g., the weight decaying parameter, the momentum factor, in the same way as in (Izmailov et al., 2018). For ImageNet, we use pre-trained models ResNet-50, ResNet-152, and DenseNet-161 contained in PyTorch to initialize  $w_0$  and fixes  $n$  to be the iteration number corresponding to 40 epochs.

The considered performance metrics include test accuracy, negative log-likelihood (NLL), and the expected calibration error (ECE) (Guo et al., 2017). The latter two are used for evaluating an algorithm’s capability for uncertainty calibration (Guo et al., 2017; Maddox et al., 2019).

In our experiments, PFGE always employs 4 model components. It uses the average of those 4 models’ softmax outputs for test-time prediction. For FGE and SWAG, we com-

pute test-time predictions by averaging softmax outputs of last 4 models that have been added into their ensemble set  $\mathcal{S}$ . By this, we guarantee that all algorithms have roughly the same overhead of model recording and test-time predictions. For reference, we also present results of FGE-whole and SWAG-whole, corresponding to FGE and SWAG that use the whole ensemble of models for test-time predictions.

### 4.2. CIFAR Datasets

We experiment with network architectures VGG16 (Simonyan & Zisserman, 2015), Preactivation ResNet-164 (PreResNet-164) (He et al., 2016b), WideResNet-28-10 (Zagoruyko & Komodakis, 2016) on CIFAR- $\{10, 100\}$ .

#### Test accuracy, NLL and ECE

We run each algorithm at least 3 times independently, and report the averaged results of test accuracy, NLL, and ECE, and the corresponding standard error in Tables 1 and 2. We bold the best-performing approach for all architectures and datasets.

On CIFAR-10, we find that for VGG16, PFGE has the highest test accuracy (93.41%). For PreResNet-164 and WideResNet-28-10, PFGE beats FGE and SWAG but loses to SWA in terms of test accuracy; SWA achieves the highest accuracy (95.78% and 96.47%) with a comparable NLL score, but gives the worst ECE score.

On CIFAR-100, we find that PFGE performs best in terms of test accuracy for all network architectures. It also gives the best NLL results for PreResNet-164 and WideResNet-28-10. SWAG gives the best calibration for VGG16. FGE gives the best calibration for PreResNet-164 and WideResNet-28-10. SWA performs worst on calibration in terms of both NLL and ECE, for all architectures.

We also find from Tables 1 and 2 that, even compared with FGE-whole and SWAG-whole, PFGE achieves a comparable even better performance in terms of test accuracy, with only 20% computational overhead of model recording and test-time predictions. The major advantage of FGE-whole and SWAG-whole lies in their capability of uncertainty calibration. They provides better NLL and ECE scores, compared with PFGE and FGE, for all architectures and datasets.

#### Reliability diagrams

We plot reliability diagrams in Figure 2, in which FGE and SWAG respectively correspond to FGE-whole and SWAG-whole in Tables 1 and 2. The result in Figure 2 re-corroborates FGE-whole and SWAG-whole’s advantage and SWA’s shortage for uncertainty calibration, and that PFGE behaves in between them in terms of calibration, for all datasets and architectures.

Table 1. Test accuracy, NLL, and ECE on CIFAR-10. The best results for each architecture are **bolded**.

Algorithm	Test Accuracy (%)			NLL (%)			ECE (%)		
	VGG16	PreResNet	WideResNet	VGG16	PreResNet	WideResNet	VGG16	PreResNet	WideResNet
PFGE	<b>93.41</b> $\pm$ 0.08	<b>95.70</b> $\pm$ 0.05	96.37 $\pm$ 0.03	26.16 $\pm$ 0.08	<b>13.05</b> $\pm$ 0.10	<b>11.04</b> $\pm$ 0.05	3.80 $\pm$ 0.08	0.54 $\pm$ 0.15	0.62 $\pm$ 0.02
FGE	93.03 $\pm$ 0.18	95.52 $\pm$ 0.08	96.14 $\pm$ 0.07	25.25 $\pm$ 0.60	13.60 $\pm$ 0.11	11.73 $\pm$ 0.15	<b>3.12</b> $\pm$ 0.09	<b>0.49</b> $\pm$ 0.09	<b>0.32</b> $\pm$ 0.08
SWA	93.33 $\pm$ 0.02	<b>95.78</b> $\pm$ 0.07	<b>96.47</b> $\pm$ 0.04	28.06 $\pm$ 0.20	13.50 $\pm$ 0.07	11.22 $\pm$ 0.11	4.44 $\pm$ 0.07	1.21 $\pm$ 0.09	11.33 $\pm$ 0.04
SWAG	93.24 $\pm$ 0.06	95.45 $\pm$ 0.14	96.36 $\pm$ 0.04	<b>24.58</b> $\pm$ 0.06	13.71 $\pm$ 0.13	11.43 $\pm$ 0.19	3.21 $\pm$ 0.03	0.75 $\pm$ 0.12	1.03 $\pm$ 0.05
FGE-whole	93.40 $\pm$ 0.08	95.57 $\pm$ 0.05	96.27 $\pm$ 0.02	21.89 $\pm$ 0.53	13.07 $\pm$ 0.10	11.18 $\pm$ 0.06	2.24 $\pm$ 0.08	0.39 $\pm$ 0.06	0.30 $\pm$ 0.08
SWAG-whole	93.37 $\pm$ 0.07	95.61 $\pm$ 0.11	96.45 $\pm$ 0.07	23.10 $\pm$ 0.29	13.12 $\pm$ 0.08	11.07 $\pm$ 0.17	3.01 $\pm$ 0.10	0.53 $\pm$ 0.09	0.78 $\pm$ 0.05

 Table 2. Test accuracy, NLL, and ECE on CIFAR-100. The best results for each architecture are **bolded**.

Algorithm	Test Accuracy (%)			NLL (%)			ECE (%)		
	VGG16	PreResNet	WideResNet	VGG16	PreResNet	WideResNet	VGG16	PreResNet	WideResNet
PFGE	<b>74.17</b> $\pm$ 0.04	<b>80.06</b> $\pm$ 0.13	<b>81.96</b> $\pm$ 0.01	132.85 $\pm$ 0.19	<b>72.07</b> $\pm$ 0.34	<b>65.00</b> $\pm$ 0.14	13.95 $\pm$ 0.07	5.05 $\pm$ 0.23	4.24 $\pm$ 0.02
FGE	73.49 $\pm$ 0.24	79.76 $\pm$ 0.06	81.09 $\pm$ 0.25	125.77 $\pm$ 0.20	72.75 $\pm$ 0.18	68.91 $\pm$ 0.18	11.80 $\pm$ 0.19	<b>3.41</b> $\pm$ 0.12	<b>2.84</b> $\pm$ 0.32
SWA	73.83 $\pm$ 0.20	79.97 $\pm$ 0.06	81.92 $\pm$ 0.02	143.23 $\pm$ 0.57	76.88 $\pm$ 0.43	69.57 $\pm$ 0.39	16.42 $\pm$ 0.29	7.56 $\pm$ 0.14	6.89 $\pm$ 0.12
SWAG	73.77 $\pm$ 0.18	79.24 $\pm$ 0.04	81.55 $\pm$ 0.06	<b>122.87</b> $\pm$ 0.88	74.37 $\pm$ 0.14	68.09 $\pm$ 0.25	<b>11.20</b> $\pm$ 0.03	4.74 $\pm$ 0.03	5.22 $\pm$ 0.07
FGE-whole	74.34 $\pm$ 0.05	80.17 $\pm$ 0.09	81.62 $\pm$ 0.16	109.93 $\pm$ 0.51	69.26 $\pm$ 0.23	63.54 $\pm$ 0.24	8.84 $\pm$ 0.01	1.92 $\pm$ 0.19	1.15 $\pm$ 0.04
SWAG-whole	74.15 $\pm$ 0.17	80.00 $\pm$ 0.03	81.83 $\pm$ 0.12	117.25 $\pm$ 0.62	71.07 $\pm$ 0.15	66.37 $\pm$ 0.29	10.99 $\pm$ 0.11	3.36 $\pm$ 0.05	4.65 $\pm$ 0.11

## Performance of separate models

We check the ensemble performance of PFGE and FGE as a function of the training iteration index  $i$ . The results of an example experiment are shown in Figure 3. We find

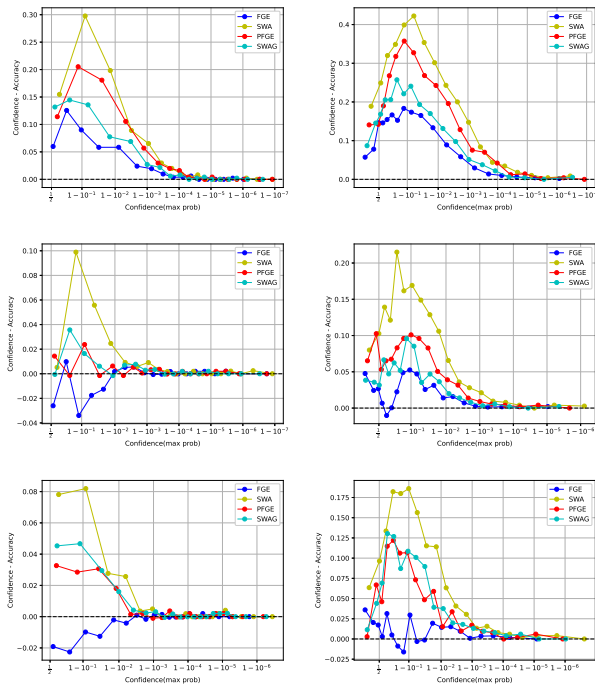


Figure 2. Reliability diagrams. Left column: CIFAR-10. Right column: CIFAR-100. Top row: VGG16. Middle Row: PreResNet-164. Bottom row: WideResNet-28-10

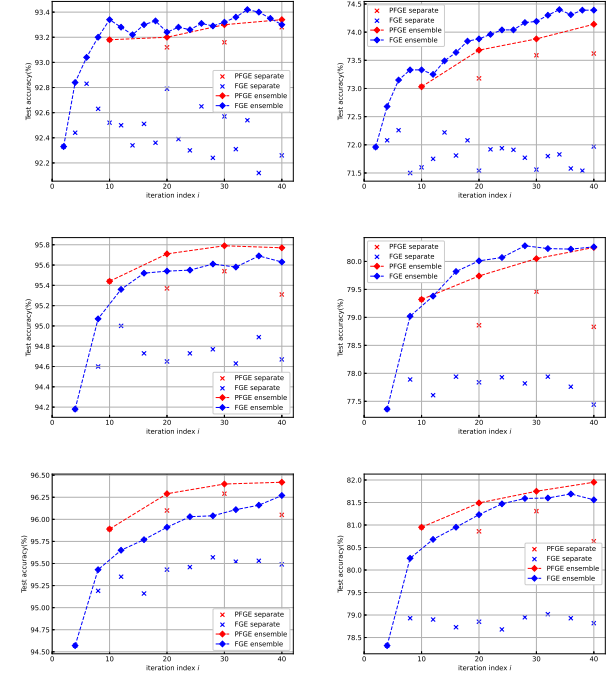


Figure 3. Ensemble performance of PFGE and FGE as a function of the training iteration index  $i$ . Crosses represent the performance of separate ‘snapshot’ models, and diamonds show the performance of the ensembles composed of all models available at the given iteration. Left column: CIFAR-10. Right column: CIFAR-100. Top row: VGG16. Middle Row: PreResNet-164. Bottom row: WideResNet-28-10.

that: (1) the separate models that construct PFGE are indeed higher-performing than those for FGE in terms of test accuracy, for all datasets and network architectures; (2) for

Table 3. Test accuracy, NLL, and ECE on Imagenet. The best results for each architecture are **bolded**.

Algorithm	Test Accuracy (%)			NLL (%)			ECE (%)		
	ResNet-50	ResNet-152	DenseNet-161	ResNet-50	ResNet-152	DenseNet-161	ResNet-50	ResNet-152	DenseNet-161
PFGE	<b>77.28</b>	<b>79.10</b>	<b>78.79</b>	<b>81.08</b>	<b>81.08</b>	<b>82.03</b>	2.00	2.61	1.84
FGE	76.77	78.71	78.45	90.47	81.91	82.87	1.59	<b>1.54</b>	<b>1.51</b>
SWA	77.13	78.84	78.75	90.90	83.40	83.47	3.43	4.10	2.46
SWAG	76.49	<b>78.75</b>	78.15	92.02	82.00	84.91	<b>1.54</b>	1.85	3.22
FGE-whole	77.25	79.08	78.84	88.62	80.21	81.31	2.19	2.43	2.54
SWAG-whole	77.09	79.04	78.66	88.94	80.19	82.85	1.73	1.65	3.35

both PFGE and FGE, the usage of more model components leads to higher test accuracy; (3) PFGE ensemble outperforms FGE ensemble in all but one cases using fewer model components. Note that the term FGE in Figure 3 corresponds to FGE-whole in Tables 1 and 2. We believe that it is the higher-quality of the separate model components that makes PFGE achieve a generalization performance comparable to FGE, with a reduced computational overhead due to the usage of fewer model components.

### Mode connectivity

In (Yang et al., 2021), the authors demonstrate that, when ensembles of trained models converge to locally smooth regions of the loss landscape, the best test accuracy is obtained. That means, the mode connectivity of its model components closely relates to the ensemble’s generalization performance. We conduct an experiment to test the mode connectivity of PFGE’s model components against that of FGE’s.

We randomly select a pair of neighboring model components, denoted by  $w$  and  $w'$ , in the ensemble set  $\mathcal{S}$ . Given  $w$  and  $w'$ , we first search a low-energy curve  $\gamma(t)$ ,  $t \in [0, 1]$ , for which  $\gamma(0) = w$ ,  $\gamma(1) = w'$ , which minimizes  $\int_0^1 \mathcal{L}(\gamma(t))dt$ , where  $\mathcal{L}$  denotes the DNN loss function. Following (Yang et al., 2021; Garipov et al., 2018), we approximate  $\int_0^1 \mathcal{L}(\gamma(t))dt$  with  $\mathbb{E}_{t \sim U(0,1)} \mathcal{L}(\gamma_\phi(t))$ , and use the Bezier curve with  $k+1$  bends, given by  $\gamma_\phi(t) = \sum_{j=0}^k \binom{k}{j} (1-t)^{k-j} t^j w_j$  for  $t \in [0, 1]$ , where  $U(0, 1)$  denotes a continuous uniform distribution between 0 and 1,  $w_0 = w$ ,  $w_k = w'$ , and  $\phi = \{w_1, \dots, w_{k-1}\}$  are parameters of additional models to be trained. Given the curve  $\gamma_\phi(t)$ , the mode connectivity of the models  $w, w'$  is defined to be (Yang et al., 2021)

$$mc(w, w') = \frac{1}{2}(\mathcal{L}(w) + \mathcal{L}(w')) - \mathcal{L}(\gamma_\phi(t^*)), \quad (1)$$

where  $t^*$  maximizes the function  $f(t) \triangleq |\frac{1}{2}(\mathcal{L}(w) + \mathcal{L}(w')) - \mathcal{L}(\gamma_\phi(t))|$ .

We use the same computational procedure and hyperparameter setting in (Yang et al., 2021; Garipov et al., 2018) to minimize the loss on the curve. We record the training loss and test error values as a function of  $t$ , and plot them in Figure 4. The related statistics is shown in Tables 4 and 5. In Figure 4, we find that the training loss curve of PFGE has a consistent lower energy than that of FGE for VGG16

and PreResNet-164. The test error curve of PFGE is below that of FGE for most  $t$  values, for all architectures. The results in Tables 4 and 5 also show a consistent advantage of PFGE over FGE in terms of both test error and training loss.

The corresponding mc values are presented in Table 6, which shows that the model connectivity of PFGE is greater than that of FGE, for all architectures.

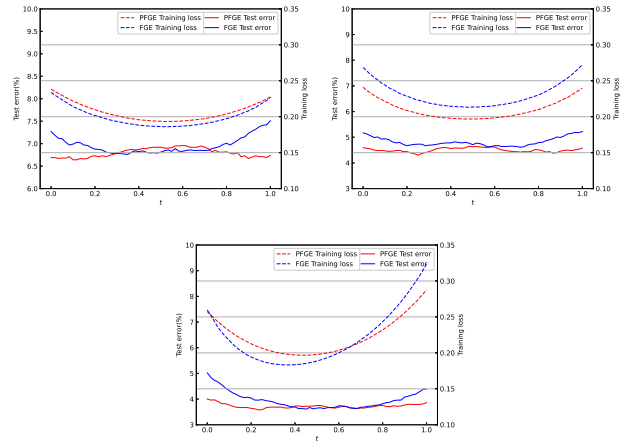


Figure 4. Test error and training loss on CIFAR-10 corresponding to  $\gamma_\phi(t)$  as a function of  $t$ . Top left: VGG16. Top right: PreResNet-164. Bottom: WideResNet-28-10.

Table 4. Statistics for test errors (%) of  $\gamma_\phi(t)$  on CIFAR-10. The test error values are collected along the changes of the  $t$  value from 0 to 1.

Architecture	Max		Min		Mean	
	PFGE	FGE	PFGE	FGE	PFGE	FGE
VGG16	6.96	7.51	6.64	6.76	6.76	6.99
PreResNet	4.65	5.22	4.30	4.61	4.50	4.82
WideResNet	4.14	4.53	3.43	3.63	3.63	3.87

Table 5. Statistics for training losses of  $\gamma_\phi(t)$  on CIFAR-10. The training loss values are collected along the changes of the  $t$  value from 0 to 1.

Architecture	Max		Min		Mean	
	PFGE	FGE	PFGE	FGE	PFGE	FGE
VGG16	0.238	0.234	0.193	0.186	0.207	0.199
PreResNet	0.241	0.272	0.197	0.213	0.210	0.230
WideResNet	0.284	0.324	0.217	0.238	0.238	0.266

Table 6. Mode connectivity test on CIFAR-10. See the definition of mc in Equation (1). A mc value closer to 0 indicates a better mode connectivity and vice versa. See more details on the relationship between the value of mc and mode connectivity in (Yang et al., 2021). The best results for each architecture are **bolded**.

Algorithm	mc value		
	VGG16	PreResNet	WideResNet
PFGE	<b>0.039</b>	<b>0.044</b>	<b>0.065</b>
FGE	0.045	0.057	0.084

### 4.3. IMAGENET

We experiment with network architectures ResNet-50 (He et al., 2016a), ResNet-152 (He et al., 2016a), and DenseNet-161 (Huang et al., 2017b) on ImageNet ILSVRC-2012 (Deng et al., 2009; Russakovsky et al., 2015). See the experimental setting in subsection 4.1.

Results in Table 3 show that PFGE outperforms FGE, SWA, and SWAG in terms of both test accuracy and NLL, and performs comparatively to FGE-whole and better than SWAG-whole in terms of test accuracy. The reliability diagrams in the left column of Figure 5 show that PFGE performs better than SWA, while worse than FGE-whole and SWAG-whole in terms of calibration. Note that the terms FGE and SWAG in Figure 5 respectively correspond to FGE-whole and SWAG-whole in Table 3. The right column of Figure 5 shows that the separate models associated with PFGE are better than those of FGE in terms of test accuracy, for all network architectures.

## 5. Conclusions

In this paper, we proposed a generic, architecture-agnostic, and highly computationally efficient ensemble-based algorithm, referred to as PFGE, to improve DNNs in terms of generalization and uncertainty calibration. In this algorithm, we use several successively performed SWA procedures to generate high-performing DNN models within the framework of FGE. We empirically demonstrated that the DNN models yielded by PFGE have better separate generalization performance and mode connectivity, compared with those of FGE. Due to these higher-performing model components, PFGE achieves better generalization performance and satisfactory calibration capability than SOTA methods, while the computational overhead of model recording and test-time predictions is significantly reduced to say 20%.

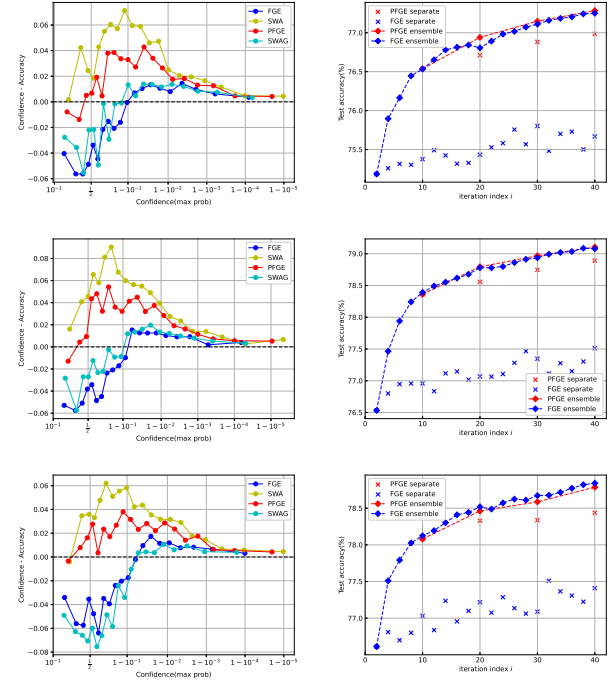


Figure 5. Left column: Reliability diagrams on Imagenet. Right column: ensemble performance of PFGE and FGE on Imagenet as a function of the training iteration index  $i$ . Top Row: ResNet-50. Middle Row: ResNet-152. Bottom Row: DenseNet-161. In subfigures of the left column, crosses represent the performance of separate “snapshot” models, and diamonds show the performance of the ensembles composed of all models available at the given iteration.

## References

Beal, J., Wu, H., Park, D. H., Zhai, A., and Kislyuk, D. Billion-scale pretraining with vision transformers for multi-task visual representations. In *Proc. of the IEEE/CVF Winter Conf. on Applications of Computer Vision*, pp. 564–573, 2022.

Bucilua, C., Caruana, R., and Niculescu-Mizil, A. Model compression. In *Proc. of the 12th ACM SIGKDD*, pp. 535–541, 2006.

Caruana, R., Niculescu-Mizil, A., Crew, G., and Ksikes, A. Ensemble selection from libraries of models. In *ICML*, pp. 18, 2004.

Chen, T., Fox, E., and Guestrin, C. Stochastic gradient Hamiltonian Monte Carlo. In *ICML*, pp. 1683–1691. PMLR, 2014.

Deng, J., Dong, W., Socher, R., Li, L., Li, K., and Fei-Fei, L. Imagenet: A large-scale hierarchical image database. In *CVPR*, pp. 248–255. Ieee, 2009.

Dietterich, T. G. Ensemble methods in machine learning. In *International workshop on multiple classifier systems*, pp. 1–15. Springer, 2000.

Duchi, J., Hazan, E., and Singer, Y. Adaptive subgradient methods for online learning and stochastic optimization. *Journal of Machine Learning Research*, 12(7), 2011.

Džeroski, S. and Ženko, B. Is combining classifiers with stacking better than selecting the best one? *Machine Learning*, 54(3):255–273, 2004.

Fort, S., Hu, H., and Lakshminarayanan, B. Deep ensembles: A loss landscape perspective. *arXiv preprint arXiv:1912.02757*, 2019.

Gal, Y. and Ghahramani, Z. Dropout as a Bayesian approximation: Representing model uncertainty in deep learning. In *ICML*, pp. 1050–1059. PMLR, 2016.

Garipov, T., Izmailov, P., Podoprikin, D., Vetrov, D., and Wilson, A. G. Loss surfaces, mode connectivity, and fast ensembling of dnns. In *Advances in Neural Information Processing Systems*, pp. 8803–8812, 2018.

Graves, A. Practical variational inference for neural networks. *Advances in Neural Information Processing Systems*, 24, 2011.

Guo, C., Pleiss, G., Sun, Y., and Weinberger, K. Q. On calibration of modern neural networks. In *ICML*, pp. 1321–1330. PMLR, 2017.

Guo, H., Jin, J., and Liu, B. Stochastic weight averaging revisited. *arXiv preprint arXiv:2201.00519*, 2022.

He, K., Zhang, X., Ren, S., and Sun, J. Deep residual learning for image recognition. In *CVPR*, pp. 770–778, 2016a.

He, K., Zhang, X., Ren, S., and Sun, J. Identity mappings in deep residual networks. In *ECCV*, pp. 630–645. Springer, 2016b.

Hinton, G., Vinyals, O., and Dean, J. Distilling the knowledge in a neural network. *arXiv preprint arXiv:1503.02531*, 2015.

Hoffman, M. D., Blei, D. M., Wang, C., and Paisley, J. Stochastic variational inference. *Journal of Machine Learning Research*, 2013.

Huang, G., Li, Y., Pleiss, G., Liu, Z., Hopcroft, J. E., and Weinberger, K. Q. Snapshot ensembles: Train 1, get M for free. In *International Conference on Learning Representations*, 2017a.

Huang, G., Liu, Z., Van Der Maaten, L., and Weinberger, K. Q. Densely connected convolutional networks. In *CVPR*, pp. 4700–4708, 2017b.

Izmailov, P., Podoprikin, D., Garipov, T., Vetrov, D., and Wilson, A. G. Averaging weights leads to wider optima and better generalization. In *Proceedings of Conference on Uncertainty in Artificial Intelligence (UAI)*, pp. 1–10, 2018.

Keskar, N. S., Mudigere, D., Nocedal, J., Smelyanskiy, M., and Tang, P. On large-batch training for deep learning: Generalization gap and sharp minima. In *International Conference on Learning Representations*, 2017.

Kingma, D. P. and Ba, J. Adam: A method for stochastic optimization. *arXiv preprint arXiv:1412.6980*, 2014.

Krizhevsky, A. and Hinton, G. Learning multiple layers of features from tiny images. *Technical report, University of Toronto*, 2009.

Kuleshov, V., Fenner, N., and Ermon, S. Accurate uncertainties for deep learning using calibrated regression. In *ICML*, pp. 2796–2804. PMLR, 2018.

Lakshminarayanan, B., Pritzel, A., and Blundell, C. Simple and scalable predictive uncertainty estimation using deep ensembles. In *Advances in Neural Information Processing Systems*, 2017a.

Lakshminarayanan, B., Pritzel, A., and Blundell, C. Simple and scalable predictive uncertainty estimation using deep ensembles. *Advances in Neural Information Processing Systems*, 30, 2017b.

Liu, B. Particle filtering methods for stochastic optimization with application to large-scale empirical risk minimization. *Knowledge-Based Systems*, 193, 2020.

Loshchilov, I. and Hutter, F. SGDR: Stochastic gradient descent with warm restarts. In *International Conference on Learning Representations*, 2017.

MacKay, D. J. C. A practical bayesian framework for back-propagation networks. *Neural computation*, 4(3):448–472, 1992.

Maddox, W. J., Izmailov, P., Garipov, T., Vetrov, D. P., and Wilson, A. G. A simple baseline for Bayesian uncertainty in deep learning. *Advances in Neural Information Processing Systems*, 32:13153–13164, 2019.

Mandt, S., Hoffman, M. D., and Blei, D. M. Stochastic gradient descent as approximate Bayesian inference. *Journal of Machine Learning Research*, 18:1–35, 2017.

Neal, R. M. *Bayesian learning for neural networks*, volume 118. Springer Science & Business Media, 2012.

Prateek, J., Sham, K., Rahul, K., Praneeth, N., and Aaron, S. Parallelizing stochastic gradient descent for least squares regression: mini-batching, averaging, and model misspecification. *Journal of Machine Learning Research*, 18, 2018.

Russakovsky, O., Deng, J., Su, H., Krause, J., Satheesh, S., Ma, S., Huang, Z., Karpathy, A., Khosla, A., Bernstein, M., Berg, A. C., and Fei-fei, L. Imagenet large scale visual recognition challenge. *International Journal of Computer Vision*, 115(3):211–252, 2015.

Schaul, T., Zhang, S., and LeCun, Y. No more pesky learning rates. In *International Conference on Machine Learning*, pp. 343–351. PMLR, 2013.

Simonyan, K. and Zisserman, A. Very deep convolutional networks for large-scale image recognition. In *ICLR*, 2015.

Smith, L. N. Cyclical learning rates for training neural networks. In *IEEE Winter Conference on Applications of Computer Vision (WACV)*, pp. 464–472. IEEE, 2017.

Sun, R. Optimization for deep learning: theory and algorithms. *arXiv preprint arXiv:1912.08957*, 2019.

Tieleman, T. and Hinton, G. Rmsprop: Divide the gradient by a running average of its recent magnitude. *Coursera: Neural Networks for Machine Learning*, 2012.

Welling, M. and Teh, Y. W. Bayesian learning via stochastic gradient langevin dynamics. In *ICML*, pp. 681–688. Citeseer, 2011.

Yang, Y., Hodgkinson, L., Theisen, R., Zou, J., Gonzalez, J. E., Ramchandran, K., and Mahoney, M. W. Taxonomizing local versus global structure in neural network loss landscapes. *Advances in Neural Information Processing Systems*, 34, 2021.

Zagoruyko, S. and Komodakis, N. Wide residual networks. In *Proc. of the British Machine Vision Conference (BMVC)*, 2016.

Zhou, Z. *Ensemble methods: foundations and algorithms*. CRC press, 2012.